Estimation of the Absolute Position of Mobile Systems by an Optoelectronic Processor

Liqiang Feng, Yeshaiahu Fainman, and Yoram Koren, *Senior Member, IEEE*

Abstract— **A method that determines the absolute position of a mobile system with a hybrid optoelectronic processor has been developed. Position estimates are based on an analysis of circular landmarks that are detected by a TV camera attached to the mobile system. The difference between the known shape of the landmark and its image provides the information needed to determine the absolute position of the mobile system. For robust operation, the parameters of the landmark image are extracted at high speeds using an optical processor that performs an optical Hough transform. The coordinates of the mobile system are computed from these parameters in a digital co-processor using fast algorithms. Different sources of position estimation errors have also been analyzed, and consequent algorithms to improve the navigation performance of the mobile system have been developed and evaluated by both computer simulation and experiments.**

I. Introduction

THE NAVIGATION of mobile systems (e.g., mobile robots [1] or automated guided vehicles [2]) relies on the fast and accurate processing of measurements needed for extracting position coordinates and range information. Since incremental measuring devices on the mobile system, such as encoders, are prone to accumulating error over distance, an absolute position estimation method is necessary. This system should operate at high speed with moderate computing power, have little or no impact on the environment, be accurate and have high flexibility (i.e., easiness of changing trajectories).

Various navigation systems have been developed, e.g., wire-guided systems [1], [3], computer vision-based systems [4]–[9], and active beacon-based systems [2], [10]–[12]. These navigation systems have certain limitations: wire-guided systems are inflexible, computer vision-based systems require high computing power and are slow in operation, active beacon-based systems require the installation of sources or sensors in the environment and may have the problem of interference between multiple mobile systems.

To overcome these limitations, many investigators have studied navigation systems based on known landmarks in the environment. Kabuka and Arenas [13] suggested the use of circular landmarks with an associated bar code to give a unique identity to each of the landmarks. Courtney, Magee and Aggarwal [5], as well as Fikui [14], used diamond-shaped landmarks and employed least-squares methods to improve the accuracy of measurements. Shyi, Lee, and Chen [15] studied navigation using triangular-shaped landmarks. The aforementioned methods are based on the geometric relationship between the landmark and its projected image detected by a camera mounted on the mobile system. A different approach was taken by Lee *et al.* [16] who used an indication post, which is a simple picture composed of different symbols and characters to provide information for the next task, e.g., the next direction of travel or distance of travel. Magee and Aggarwal [7] used a single sphere with horizontal and vertical calibration great circles as a landmark, Sugihara [8] and Krotkov [9] used prestored map with landmarks and computer vision techniques to detect the edge of the landmark, and then determine the position and orientation of the robot.

All of these approaches are based on digital computation in which the processing time at each location is on the order of seconds (0.5–20 s), depending on the complexity of the algorithms employed. Certainly, this computing speed is slow for the real-time operation of fast mobile systems. To increase the computing speed, we introduce a hybrid optoelectronic computing system for landmark navigation. The hybrid optoelectronic implementation allows us to achieve high processing speeds for real-time operation (at the frame rate of 1/30 s).

To improve the accuracy and reliability of position estimation, data fusion techniques have been used. The basic idea is to use sensory information from different sensors (same kind or different kinds) to obtain better position estimation. Many researchers have worked on this subject. Wang [17] presented an uncertainty analysis about the location estimation, McKendall and Mintz [18] utilized statistical decision theory to formulate the problem of location data fusion, Luo *et al.* [19] developed a dynamic multisensor data fusion system for intelligent robots, Durrant-Whyte [20] emphasized the sensor model and its role in multisensor integration, Flynn [21] studied the problem of combining sonar and infrared sensors for mobile robot navigation, Richardson and Marsh [22] studied problems of fusionability of different sensory data and desirability of sensor fusion, and Smith and Cheeseman [23] addressed the problem of error propagation in coordinate transformation.

In our case, the position information comes from two sources: the wheel encoders that generate incremental position measurements and the landmark that provide absolute posi-

Manuscript received August 5, 1990; revised February 2, 1992. This work is supported in part by CAMRSS (a NASA Center for Commercial Development of Space), and in part by the Department of Energy grant DE-FG02-86NE37969, which supports a multiuniversity project.

L. Feng and Y. Koren are with the Mobile Robot Laboratory, Department of Mechanical Engineering and Applied Mechanics, The University of Michigan, Ann Arbor, MI 48109-2125.

Y. Fainman is with the Department of Electrical and Computer Engineering, University of California, San Diego, La Jolla, CA 92093.

IEEE Log Number 9201422.

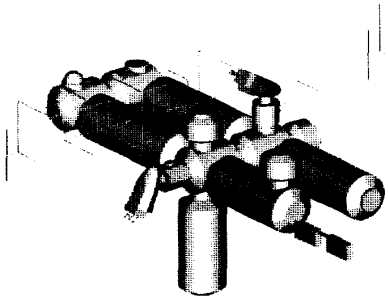

Fig. 1. Space station.

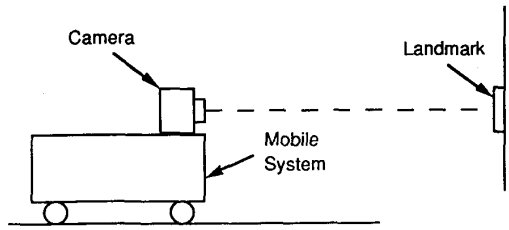

Fig. 2. Mobile system and a landmark.

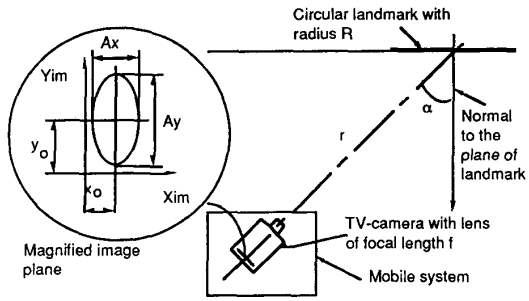

Fig. 3. Description of the relative spatial position of the mobile system and a landmark.

tion measurements. The position information obtained from the incremental measurements can be accurate over a short distance, but the error will accumulate over the distance. On the other hand, the absolute position measurements have bounded error, but their accuracy depends on the relative position between the robot and the landmark. Clearly, if we can combine the information from these two sources, we can obtain a better position estimate. In this paper, we will develop several data fusion algorithms for these two sources of sensory data by employing statistical modeling techniques and different statistical optimization criteria.

In Section II, we will discuss the operational principles of the proposed mobile system and describe the hybrid optoelectronic processing approach. In Section III, we will discuss the positioning errors, and in Section IV, we will develop a number of algorithms that improve the performance of the mobile system. In Section V, we will provide computer simulations and experimental results. The final conclusions are given in Section VI.

II. The Hybrid Optoelectronic Processor

In this section, we will introduce the navigation algorithm based on landmarks and describe its implementation using the hybrid optoelectronic processor.

A. Operational Principles

The navigation algorithm is based on the analysis of known landmarks (i.e., parametric curves such as lines and circles) that are artificially introduced or naturally exist in the environment. For example, the circles and the rectangular shapes on the spacecraft depicted in Fig. 1 are natural landmarks. The image of the landmark is detected by a TV camera mounted on the mobile system. The shape of this image depends on the relative orientation of the TV camera to the landmark. In this paper, we consider 2-D landmark navigation in which the axis of the camera lens lies in a plane perpendicular to the plane of the landmark and the center of the camera lens is at the same height as the center of the landmark. In this case, we need only two coordinates to determine the relative position of the mobile system with respect to the landmark (see Fig. 2). When a circle is used as a landmark, the TV image will be an ellipse. Four parameters (i.e., two axes and the two coordinates of the center) are needed to determine the ellipse completely.

In the case where the camera is pointing at the center of the circle, the relative coordinates of the mobile system to a circular landmark (see Fig. 3) are determined by

$$r = \frac{fR}{A_y}$$
$$\cos\alpha = \frac{fr - \sqrt{f^2r^2 - 4A_x^2(r^2 - R^2)}}{2A_xR} \tag{1}$$

where r and α are the polar coordinates of the mobile robot system with respect to the landmark, A_x and A_y are the axes of the ellipse in the image plane (the coordinates of the ellipse center x_0 and y_0 are both zero), R is the radius of the circular landmark, and f is the focal length of the TV camera lens. The detailed derivation of (1) is given in Appendix I. In the general 2-D case (i.e., when the camera is not pointing at the center of the circle), the ellipse will be shifted, and r and α will depend on f, R, A_x, A_y, and x_0.

B. Hybrid Optoelectronic Processor

A block diagram of the hybrid optoelectronic processor is shown in Fig. 4. The image of the landmark (e.g., ellipse) is detected by a TV camera, transmitted to the optical processor where time-consuming operations and transformations are performed at high speed, and received there by the electronic-to-optical interface (i.e., a liquid crystal display device). The parameters of the ellipse are determined at very high speed by computing the Hough transform optically [24]. The output of the optical processor (i.e., the Hough transform parameter domain) is detected by the CCD arrays and is introduced to the digital electronic microprocessor. This microprocessor is used to analyze the output, determine the relative coordinates using (1), and provide control signals for navigation of the mobile system.

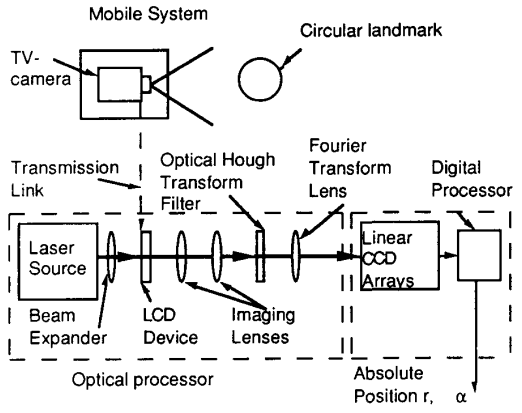

Fig. 4. Block diagram of the hybrid optoelectronic processor.

The Hough transform (HT) is a space-variant transform that maps the input image plane to a parameter domain plane [24]. To detect the parameters of a straight line in normal parameterization, each point in the image plane (x, y) is transformed into a sinusoidal curve in the parameter domain according to

$$\rho = x\cos\theta + y\sin\theta \tag{2}$$

where (θ, ρ) are the coordinates of the HT parameter domain. Note that the parameters of a straight line in the image plane are represented by the coordinates of a point in the HT parameter domain.

The amplitude distribution of the light in the parameter domain, $F(\theta, \rho)$, is related to the amplitude distribution of the light in the input plane, $f(x, y)$, according to

$$F(\theta,\rho) = \int_{-\infty}^{\infty}\int_{-\infty}^{\infty} f(x,y)\delta(\rho - x\cos\theta - y\sin\theta)dxdy \tag{3}$$

where $\delta(\rho - x\cos\theta - y\sin\theta)$ is the point spread function (PSF) that corresponds to an input point (x,y) and the output sinusoidal curve $\rho = x\sin\theta + y\cos\theta$.

An ellipse in the image plane (x, y) may be described by the parametric equations

$$\begin{aligned} x &= x_0 + A_x\cos\beta \\ y &= y_0 + A_y\sin\beta \end{aligned} \tag{4}$$

where A_x and A_y are the two axes, x_o and y_o are the coordinates of the center of the ellipse, and β is a parameter $(0 \leq \beta \leq 2\pi)$. Thus, A_x, A_y, x_o and y_o are the four parameters that characterize the ellipse. Equation (2) can be rewritten for an ellipse as

$$\rho = (x_0 + A_x\cos\beta)\cos\theta + (y_0 + A_y\sin\beta)\sin\theta. \tag{5}$$

The amplitude distribution of light in the parameter domain (see (3)) consists of a superposition of curves described by (5) with β varying from 0 to 2π. The margins of the superposition of the sinusoidal curves in the parameter domain create an envelope. Since ρ is a function of both θ and β for any given curve segment, the envelopes of the HT in the (θ, ρ) domain

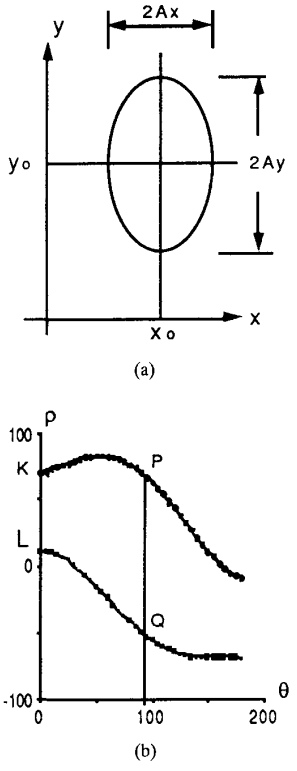

Fig. 5. Extraction of the parameters of an ellipse using the Hough transform. (a) Input ellipse image. (b) Output image from the HT envelope, using a HT filter with an impulse response for the detection of a straight line in normal parameterization.

will correspond to the extreme values obtained by varying β at each θ, i.e., from the equation $\partial\rho/\partial\beta = 0$. This results in

$$\tan\beta = \frac{A_y\tan\theta}{A_x}. \tag{6}$$

By substituting (6) into (5), we obtain two envelopes, one upper and one lower:

$$\rho_{\text{envelope}} = x_0\cos\theta + y_0\sin\theta \pm \sqrt{A_x^2\cos^2\theta + A_y^2\sin^2\theta}. \tag{7}$$

The HT of the ellipse expressed by (4) yields an image in the parameter domain that is described by these sinusoidal envelopes, as shown in Fig. 5.

The parameters of the ellipse can be extracted from the amplitude distribution of the light in the HT domain along two lines: $\theta = 0°$ and $\theta = 90°$ [24]. An appropriate substitution of θ into (7) yields the coordinates ρ of points K, L, P, and Q (shown in Fig. 5) which are given by $(0°, x_0 + A_x), (0°, x_0 - A_x), (90°, y_0 + A_y)$, and $(90°, y_0 - A_y)$, respectively. These coordinates are detected and used to extract the parameters of the ellipse:

$$\begin{aligned} x_0 &= \frac{\rho_K + \rho_L}{2} & y_0 &= \frac{\rho_P + \rho_Q}{2} \\ A_x &= \frac{\rho_K - \rho_L}{2} & A_y &= \frac{\rho_P - \rho_Q}{2}. \end{aligned} \tag{8}$$

To expand the 2-D case to the more general 3-D case, we have to determine one more parameter that corresponds to the

rotation of the ellipse. This can be accomplished by analyzing the HT plane along an additional line, θ = constant. This additional measurement will allow us to determine the phase of the envelope in Fig. 5, thus providing information on the fifth parameter, the rotation of the ellipse.

There are several advantages for detecting the parameters of the image in the HT domain. First, since with our method we need to measure the coordinates only along a few lines (in the 2-D case, only two lines), there is no need to introduce the whole image into the computer as done in other landmark based methods [7]–[9], [13]–[15]. This saves data transmission time and memory. Secondly, when part of the landmark is occluded (i.e., not visible), we can not use the method described in [13]. By contrast, in the HT domain, the resultant envelopes are built from the contributions of all the points on the ellipse, so even some points are missing in the image, there is still enough information in the HT domain that will allow us to extract the ellipse parameters.

When implemented in a general purpose computer, the Hough transform is quite time and memory consuming, it is very difficult to achieve real time requirement without special parallel processor. Optical Hough transform takes the advantages of parallel processing and large memory capacity of the hologram to make the Hough transform practical for robot navigation application. Furthermore, the new approach has the potential to employ optical pattern recognition techniques to incorporate a finite number of landmarks of different shapes to increase the flexibility. For example, in the image domain, we can use optical pattern matching to distinguish different landmarks, and in the HT domain, we can use line detection to detect rectangular landmarks.

III. Error Analysis

The precision of landmark-based navigation depends on errors caused by the measurement system and the mobile system. The limited resolution of the TV camera, the CCD arrays and the Hough transform filter, affects the measurement accuracy, and imperfections of the mechanical system, as well as environmental factors, cause deviations of the mobile system. These two kinds of errors are analyzed below.

The measurement error is mainly determined by the digitization error, which occurs due to the limited resolution of the TV camera, the CCD arrays, and some optical devices (e.g., the liquid crystal display and the Hough transform filter). It is dominated by the lowest resolution of these devices. The minimum measurement error due to digitization can be determined from the size of the detected image and the detector resolution. For example, for a TV camera that permits the resolution images the size of 512×512 pixels, this error is on the order of $1/512 = 0.002$. But if the image does not occupy the full TV frame, the measurement error is larger.

The measurement error is also affected by sensitivity functions that are defined as the ratio of the change in the position of the mobile system to the change in the image parameters, namely, $\partial r/\partial A_x$, $\partial r/\partial A_y$, $\partial \alpha/\partial A_x$, and $\partial \alpha/\partial A_y$. The sensitivity functions are not fixed, and they depend on the relative position of the mobile system to the landmark. The sensitivities measure how sensitive are the position estimation to the measurement error ΔA_x and ΔA_y. In general, the mobile system's polar coordinates r and α are functions of the measurements A_x and A_y (see (1)); therefore, the position error Δr and $\Delta \alpha$ can be expressed by

$$\begin{aligned}\Delta r &= \frac{\partial r}{\partial A_x}\Delta A_x + \frac{\partial r}{\partial A_y}\Delta A_y \\ \Delta \alpha &= \frac{\partial \alpha}{\partial A_x}\Delta A_x + \frac{\partial \alpha}{\partial A_y}\Delta A_y \end{aligned} \tag{9}$$

where ΔA_x and ΔA_y are the measurement errors of the two axes of the ellipse and are determined by the digitization error. In real situations, the digitization error is a function of the relative position and the resolution of the devices. The coefficients, or sensitivities, $\frac{\partial r}{\partial A_x}$, $\frac{\partial r}{\partial A_y}$, $\frac{\partial \alpha}{\partial A_x}$, and $\frac{\partial \alpha}{\partial A_y}$ are functions of the relative position of the mobile system to the landmark.

The sensitivities can be determined from (1) which may be rewritten in the following form:

$$\begin{aligned}A_x &= \frac{fRr\cos\alpha}{r^2 - R^2\sin^2\alpha} \\ A_y &= \frac{fR}{r}.\end{aligned}$$

In practice, the distance between the mobile system and the landmark r is much larger than the radius of the circular landmark R, so the previous equations can be approximated as

$$\begin{aligned}A_x &\approx \frac{fR\cos\alpha}{r} \\ A_y &= \frac{fR}{r}.\end{aligned} \tag{10}$$

We can now solve for r and α:

$$\begin{aligned}r &= \frac{fR}{A_y} \\ \alpha &= \arccos\frac{A_x}{A_y}.\end{aligned} \tag{11}$$

The sensitivity functions of the relative position of the mobile system with respect to the landmark are derived from (11); after substituting (10), we obtain

$$\begin{aligned}\frac{\partial r}{\partial A_x} &= 0 \\ \frac{\partial r}{\partial A_y} &= -\frac{r^2}{fR} \\ \frac{\partial \alpha}{\partial A_x} &= -\frac{r}{fR\sin\alpha} \\ \frac{\partial \alpha}{\partial A_y} &= \frac{r\cos\alpha}{fR\sin\alpha}.\end{aligned} \tag{12}$$

The approximated positioning errors are obtained by substituting (12) into (9):

$$\begin{aligned}\Delta r &= -\frac{r^2}{fR}\Delta A_y \\ \Delta \alpha &= -\frac{r}{fR\sin\alpha}\Delta A_x + \frac{r\cos\alpha}{fR\sin\alpha}\Delta A_y.\end{aligned} \tag{13}$$

TABLE I

Real		Measured		Calculated		Error	
r	α	A_x	A_y	r_m	α_m	$\Delta r/r_m$	$\Delta\alpha/\alpha_m$
4000	15	56	75	4028	10.86	0.7%	−27.6%
4000	45	41	75	4028	43.62	0.7%	−3.1%
4000	75	15	75	4028	72.93	0.7%	−2.76%
2000	45	82	151	2003	45.47	0.2%	1.04%

From (12), we can observe that all the sensitivity functions increase with an increase in r. We can also see that if r is kept constant, the sensitivities with respect to α decrease with an increase in α, and the sensitivities with respect to r do not depend on α.

Assuming we have constant digitization errors ΔA_x and ΔA_y, we can observe that for a mobile system moving away from the landmark under a certain orientation, the measurement errors Δr and $\Delta\alpha$ increase due to the increase in r. If we keep a fixed distance between the mobile system and the landmark, but change the angle of view α, the measurement error $\Delta\alpha$ decreases with the increase in α, and Δr does not change. In some special cases, when $\alpha = 0°$, there is no information on α; therefore, the error in α tends to infinity, i.e., $\Delta\alpha \to \infty$. When α goes near 90°, from (10), we can see that $A_x \to 0$, the measurement error becomes significant. When $r \to \infty$, the errors in both r and α tend to infinity.

Simple experiments have been conducted to evaluate the effects of digitization and sensitivity on the accuracy of position measurements. The results are summarized in the Table I. The experimental results in Table I are consistent with the analysis discussed previously.

To improve the measurement accuracy, we will introduce a statistical model for the digitization error by assuming that the image parameters are random variables that possess a normal distribution. The probability model will allow us to employ statistical techniques to improve the navigation of the mobile system.

The variances of the position estimates are functions of the digitization error and the sensitivity. The errors in determining the coordinates of the mobile system depend on the digitization error and the sensitivity, according to (9). By assuming that A_x and A_y are normally distributed independent random variables, we then know the linear combination of Gaussian variables is also a Gaussian random variable, and the variances of the coordinates are related to the variances of A_x and A_y by [25]

$$\sigma_r^2 = \left(\frac{\partial r}{\partial A_x}\right)^2\sigma_{A_x}^2 + \left(\frac{\partial r}{\partial A_y}\right)^2\sigma_{A_y}^2$$
$$\sigma_\alpha^2 = \left(\frac{\partial \alpha}{\partial A_x}\right)^2\sigma_{A_x}^2 + \left(\frac{\partial \alpha}{\partial A_y}\right)^2\sigma_{A_y}^2 \tag{14}$$

where $\sigma_{A_x}^2$ and $\sigma_{A_y}^2$ are the variances of the two axes of the ellipse, and σ_r^2 and σ_α^2 are the variances of the coordinates of the mobile system.

The positioning accuracy of mobile systems is affected by factors of the mobile system and the environment. In many mobile systems only indirect incremental position transducers are employed such as incremental encoders in wheeled mobile robots. In these cases, position errors exist due to the different diameters of the wheels, wheel misalignment and asymmetric vehicle loads, as well as the floor conditions that may be different for different wheels [26], [27]. Since the positioning errors caused by these factors can not be detected by the encoders, the errors accumulate over the distance. Obviously, an absolute position measuring method becomes essential for reliable navigation.

IV. Algorithms for Improved Performance

The simplest way to combine absolute and incremental measurements, is to use last absolute measurement at point i as a reference and add to it the incremental readings between point i and $i+1$, where the next absolute measurement is taken. This method, however, is very sensitive to errors in the absolute measurement at point i. A more accurate system may be one in which information from previous measurements is also utilized. In this section, we will develop algorithms that use the present and previous measurements of the landmark as well as the encoder readings of the mobile system to improve the navigation accuracy.

When the mobile system is instructed to move, measurements are taken at different points along the trajectory. At each point, a new estimate of the current position is obtained based on the new as well as previous measurements. Each previous measurement is projected to the present vehicle location according toe following equation:

$$x_i^n = x_i^i + \sum_{j=i}^{n-1} \Delta x_j^{j+1} \tag{15}$$

where x_i^i is the landmark measurement at point i, Δx_j^{j+1} is the increment from point j to point $j-1$, which is obtained from the readings of the encoders, and x_i^n is the projection to point n from the measurement at point i. In our discussion, x is used as a general variable, and it represents either r or α.

In developing the navigation algorithms, we will consider two errors, the landmark measurement error and the mobile system error. The measurement error is caused by the limited resolution of the devices and is sensitive to the location of the mobile system (see (13)). In order to increase the robustness and positioning accuracy of the mobile system, we will use algorithms based on a weighted average method [28]:

$$\bar{x}^n = \frac{\sum_{i=1}^n w_i x_i^n}{\sum_{i=1}^n w_i} \tag{16}$$

where $\bar{x}^n$ is the new estimate of the current position at point n, x_i^n is the predicted point n position based on measurement at point i according to (15), and w_i is the weight that gives the optimal estimate (see Section IV-A). The weighted average is used to fuse the information from both the new measurement and the projections from previous measurements ((15)) to get a better position estimation. Equation (16) can be also rewritten in the recursive form:

$$\bar{x}^n = \bar{x}_{n-1}^n + \frac{w_n(x_n^n - \bar{x}_{n-1}^n)}{\sum_{i=1}^n w_i} \tag{17}$$

where $\bar{x}_{n-1}^n$ is the projection from the last estimate, i.e., $\bar{x}_{n-1}^n = \bar{x}^{n-1} + \Delta x_{n-1}^n$ and x_n^n is the new measurement at point i.

To counteract for the mobile system error, we must realize that the errors caused by the imperfection of the mobile system itself and the environmental factors accumulate over distance. In order to avoid the buildup of large errors, we use a *moving window* to include only the most recent measurements into the weighted average process. In Section IV-B, we will discuss the situation where both measurement and mobile system errors present.

A. Compensating for the Measurement Error due to Sensitivity

If the mobile system errors are small, the major source of error will be the measurement error. We will develop algorithms based on the weighted average of (16) to compensate for the measurement error based on different optimization criteria.

Algorithm with Weights Based on Sensitivity: The sensitivity of measuring the landmark parameters depends on the location of the mobile system, as shown in (11). In general, the accuracy of the measurement decreases with an increase in sensitivity, i.e., a measurement obtained in a low sensitivity region is more reliable and should be assigned a larger weight. From (9), we can see that if we assume a constant digitization error, the measurement error depends only on sensitivities. Thus, selecting the weights of the weighted average based on sensitivities might be an appropriate approach (under the assumption of a constant digitization error, an assumption that is hard to justify).

The sensitivities given in (11) are used as the weights in (16). Since $(\partial\alpha/\partial A_x) = 0$ and $(\partial\alpha/\partial A_x) \geq (\partial\alpha/\partial A_y)$, the dominant sensitivity factors become $\partial r/\partial A_y$ and $\partial\alpha/\partial A_x$. We take $w_\alpha = 1/(\partial\alpha/\partial A_x)$ and $w_\alpha = 1/(\partial r/\partial A_y)$, and the estimated location of the mobile system is calculated using the following equations:

$$\bar{r}^n = \frac{\sum_{i=1}^n w_i^r r_i^n}{\sum_{i=1}^n w_i^r}$$
$$\bar{\alpha}^n = \frac{\sum_{i=1}^n w_i^\alpha \alpha_i^n}{\sum_{i=1}^n w_i^\alpha} \tag{18}$$

where $\bar{r}^n$ and $\bar{\alpha}^n$ are the estimated distance and the orientation of the mobile system, respectively; w_i^r and w_i^α are the weights at point i, and r_i^n and α_i^n are the projections for the coordinates at point n, which are defined by equations similar to (15).

Equation (18) can be expressed in the following recursive form:

$$\bar{r}^n = \bar{r}_{n-1}^n + \frac{w_n^r(r_n^n - \bar{r}_{n-1}^n)}{\sum_{i=1}^n w_i^r}$$
$$\bar{\alpha}^n = \bar{\alpha}_{n-1}^n + \frac{w_n^\alpha(\alpha_n^n - \bar{\alpha}_{n-1}^n)}{\sum_{i=1}^n w_i^\alpha} \tag{19}$$

where r_n^n and α_n^n are the new measurements, and $\bar{r}_{n-1}^n$ and $\bar{\alpha}_{n-1}^n$ are the projections from the last estimate, i.e, $\bar{r}_{n-1}^n = \bar{r}^{n-1} + \Delta r_{n-1}^n$ and $\bar{\alpha}_{n-1}^n = \bar{\alpha}^{n-1} + \Delta\alpha_{n-1}^n$. An evaluation of this algorithm and comparisons to those presented in the following subsection are given in Section V.

Minimizing the Variance of the New Estimate: The algorithm described by (18) is not based on an optimization procedure. In contrast, our second algorithm is based on minimizing the variance of the new estimate. Assuming that x_i^n in (16) are independent random variables, we can determine the variance of every new estimate by [28]:

$$\sigma_{\bar{r}^n}^2 = \frac{\sum_{i=1}^n (w_i^r)^2 \sigma_{r_i}^2}{(\sum_{i=1}^n w_i^r)^2} \tag{20}$$

where $\sigma_{r_i^n}^2$ is the variance of the projection of r from point i, and $\sigma_{\bar{r}^n}^2$ is the variance of the new estimate of the distance at point n.

In order to minimize the variance, we must satisfy the relation

$$\frac{\partial\sigma_{\bar{r}^n}^2}{\partial w_i^r} = 0. \tag{21}$$

Substituting (20) into (21) and solving the resultant equation, we obtain the optimum weights [28]:

$$w_i^r \propto \frac{1}{\sigma_{r_i^n}^2}. \tag{22}$$

A similar relation can be obtained for the second coordinate α: $w_i^\alpha \propto 1/(\sigma_{\alpha_i^n}^2)$. This result can also be obtained by applying a Kalman filter [30].

Minimizing the Mean Square Error of the New Estimate: The third algorithm is based on minimizing the mean square error of the new estimate. The mean square error at point n can be expressed by

$$J = \sum_{i=1}^n (\bar{r}^n - r_i^n)^2 \tag{23}$$

where $\bar{r}^n$ is the estimate for point n given by (16), and r_i^n is the projection to point n from point i. To minimize the error, we have to satisfy the following equation:

$$\frac{\partial J}{\partial w_i^r} = 0 \tag{24}$$

where $i = 1, \cdots, n-1$. Substituting (23) and (16) into (24), we obtain

$$\sum_{i=1}^n w_i^r (r_i^n - r_j^n) = 0 \tag{25}$$

where $j = 1, 2, \cdots, k-1, k+1, \cdots, n-1$. Assuming a certain value for the kth weight, w_k^r, we can rewrite the last equation as

$$\begin{bmatrix} 0 & r_2^n - r_1^n & r_3^n - r_1^n & \cdots & r_n^n - r_1^n \\ r_1^n - r_2^n & 0 & r_3^n - r_2^n & \cdots & r_n^n - r_2^n \\ \cdots & & & & \\ r_1^n - r_n^n & r_2^n - r_n^n & r_3^n - r_n^n & \cdots & 0 \end{bmatrix} \begin{bmatrix} w_1^r \\ w_2^r \\ \cdots \\ w_n^r \end{bmatrix} = w_k^r \begin{bmatrix} r_1^n - r_k^n \\ r_2^n - r_k^n \\ \\ r_n^n - r_k^n \end{bmatrix}. \tag{26}$$

By solving this system of linear equations at each point, we find the optimal weights for minimizing the mean square error

of the new estimate at this point. To avoid the trivial solution of this homogeneous linear system, we must first pick one weight. The weight in the highest sensitivity region is assigned a weight of 1, or $w_k^r = 1$. The derivation of (26) is given in Appendix II.

Considering the real-time requirements of the navigation problem, we adopt the recursive least-squares algorithm for (26) [30], which solves the least-squares problem approximately by using a recursive relation at each point:

$$\bar{r}^n = \bar{r}_{n-1}^n + \frac{a_{n-1}(r_n^n - \bar{r}_{n-1}^n)}{P_{n-1}}$$
$$P_i = P_{i-1} - \frac{a_i P_{i-1}^2}{1 + a_i P_{i-1}} \tag{27}$$

where r_n^n is the new measurement, $\bar{r}_{n-1}^n$ is the projection from the last estimate, $\bar{r}^n$ is the new estimate, a_i is the weight, and P_i is a variable gain, which can start with an arbitrary positive value. Equations similar to (27) can be obtained for α.

B. Compensating for Both Measurement and Mobile System Errors

In the three algorithms discussed in Section IV-A, we used the previous absolute measurements and the encoder readings to estimate the new positions. However, as discussed in Section III-B, there could be a large accumulation of errors in the encoder readings due to the mobile system errors (e.g., different sized tire, slippery floors, or misaligned wheels). To reduce the effect of incremental error accumulation, we adopted the strategy of introducing a moving window. With this strategy, the effect of the previous measurements on the current position estimate diminishes over the distance. In this study, we use the weighted average of the current measurement and the projected estimate from the last measurement.

We will use a weighted average for two successive measurements and select the weights such that the resultant new estimate will have the minimum variance. If we assume that the random variables r and Δr are independent, we have

$$\bar{r}^n = \frac{w_n^r r_n^n + w_{n-1}^r(\bar{r}^{n-1} + \Delta r_{n-1}^n)}{w_n^r + w_{n-1}^r} \tag{28}$$

$$\sigma_{\bar{r}^n}^2 = \left(\frac{w_n^r}{w_n^r + w_{n-1}^r}\right)^2 \sigma_{r_n^n}^2 + \left(\frac{w_{n-1}^r}{w_n^r + w_{n-1}^r}\right)^2 \left(\sigma_{\bar{r}^{n-1}}^2 + \sigma_{\Delta r_{n-1}^n}^2\right) \tag{29}$$

where $\sigma_{\bar{r}^n}^2$ is the variance of the new estimate, $\sigma_{r_n^n}^2$ is the variance of the new measurement, $\sigma_{\bar{r}^{n-1}}^2$ is the variance of the estimate at the previous position, and $\sigma_{\Delta r_{n-1}^n}^2$ is the variance of the increment Δr_{n-1}^n. To minimize the variance of the new estimate, we compute the derivative of $\sigma_{\bar{r}^n}^2$ with respect to w_{n-1}^r using (29):

$$\frac{\partial \sigma_{\bar{r}^n}^2}{\partial w_{n-1}^r} = 0. \tag{30}$$

We solve (30) for w_{n-1}^r and obtain

$$w_{n-1}^r = \frac{w_n^r \sigma_{r_n^n}^2}{\sigma_{\bar{r}^{n-1}}^2 + \sigma_{\Delta r_{n-1}^n}^2}. \tag{31}$$

By substituting (31) into (28) and (29), we obtain

$$\sigma_{\bar{r}^n}^2 = \frac{(\sigma_{\bar{r}^{n-1}}^2 + \sigma_{\Delta r_{n-1}^n}^2)\sigma_{r_n^n}^2}{\sigma_{\bar{r}^{n-1}}^2 + \sigma_{\Delta r_{n-1}^n}^2 + \sigma_{r_n^n}^2} \tag{32}$$

$$\bar{r}^n = \frac{(\sigma_{\bar{r}^{n-1}}^2 + \sigma_{\Delta r_{n-1}^n}^2) r_n^n + \sigma_{r_n^n}^2(\bar{r}^{n-1} + \Delta r_{n-1}^n)}{\sigma_{\bar{r}^{n-1}}^2 + \sigma_{\Delta r_{n-1}^n}^2 + \sigma_{r_n^n}^2}. \tag{33}$$

We can see from (33) that the weights are still inversely proportional to the variance, but when the new measurement is more accurate (i.e., $\sigma_{\bar{r}^n}^2 < \sigma_{\bar{r}^{n-1}}^2 + \sigma_{\Delta r_{n-1}^n}^2$), a larger weight is obtained for the new measurement. Otherwise, a larger weight is obtained for the projection from the last estimate.

In the ideal situation, i.e., $\sigma_{\Delta r_{n-1}^n}^2 = 0$, $(k = 0, 1, \cdots, n)$, all the measurements are of the same accuracy, $\sigma_{r_k^k}^2$, $(k = 0, 1, \cdots, n)$, and the best estimate should be the arithmetic average. We can show that under these assumptions, (33) indeed will reduce to the simple arithmetic average.

C. The Computational Complexity of the Algorithms

The proposed algorithm employs the optical processing to implement the time consuming Hough transform, then uses a digital computer to compute the position and orientation and enhance the precision with the aid of data fusion algorithms. Without these algorithms, the computational time is at the order of a few microseconds. All the data fusion algorithms developed in Section IV are recursive weighted average algorithms with very short computational cycles. Even the most complicated algorithm introduced in Section IV-B requires only the calculation of the coordinates r and α from (1), variances of the coordinates r and α from (12) and (14), and the estimated coordinates $\bar{r}$ and $\bar{\alpha}$ from (32) and (33). So the numerical calculations required at each step are rather simple (take less than 1 ms on a 386 computer). Therefore the processing time required at each step is dominated by the video frame rate which is about 30 ms. While the digital implementation of the same scheme will take much longer (in the order of seconds).

V. Simulations and Experimental Results

We have performed computer simulations and experimental evaluations of the proposed hybrid optoelectronic navigation system using the different algorithms introduced in Section IV. The results are summarized below.

A. Computer Simulations

The objective of this computer simulation is to verify the effectiveness of the algorithm developed in Section IV-B when both measurement and mobile system errors are present. In the simulation, the mobile system moves along a straight path with incremental steps of 200 mm. Measurements are taken at each step (12 steps total). At the target point, a new estimate

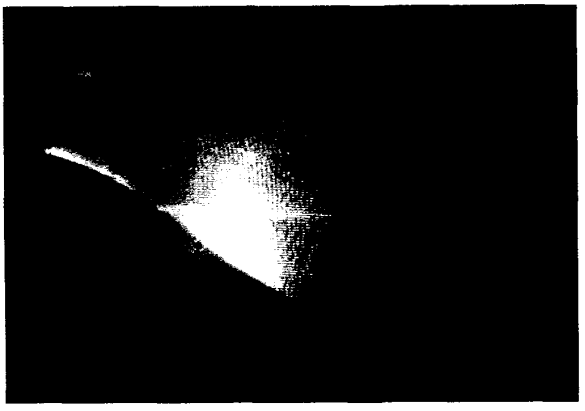

Fig. 6. Typical output from the optical processor.

of the current position is obtained using the new as well as the previous measurements with the weighting factors of the different algorithms. The data from the encoders of the mobile system are also used. The final correction is then made toward the target based on the new position estimation.

We introduced a mobile system error of 10% for two simulation cases: 1) a mobile system error occurs only at the second step; and 2) a mobile system error occurs only at the 10th step, where the total number of steps is 12. We have chosen these two cases to demonstrate the effectiveness of the algorithm in controlling errors that occur at the beginning of the route and at its end. The results of the computer simulation for the two cases are summarized in Fig. 7(a) and (b), respectively. In each case, errors at the target point are compared for three navigation strategies: 1) motion based on the new measurement; 2) motion based on the algorithm that minimizes the variance of the new estimate without a moving window; and 3) motion based on the algorithm in 2) but using a moving window.

From the results in Fig. 7, we observe that 1) the algorithm based on minimizing the variance of the new estimate with a moving window gives the best performance; 2) the mobile system error has a significant effect on the position estimation; and 3) a moving window is an effective way of compensating for error accumulation.

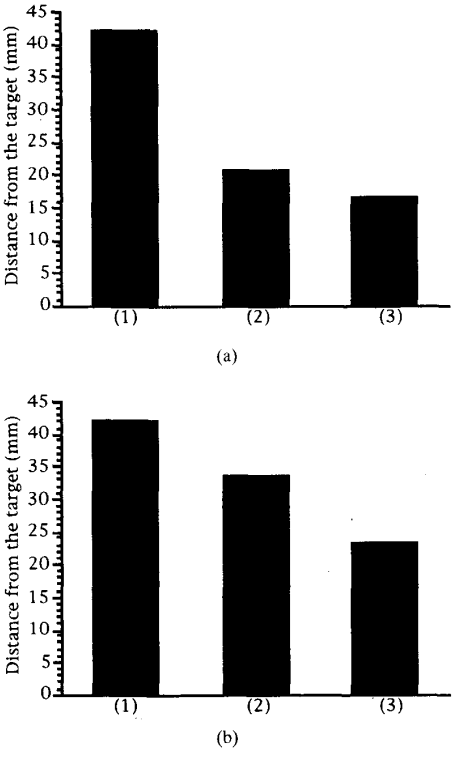

Fig. 7. Comparisons of computer simulations of the navigation errors for different correction criteria: (a) mobile system gives an error only at the second step; (b) mobile system gives an error only at the 10th step, where the total number of steps is 12. In each plot, from left to right, motion is based 1) only on the new measurement; 2) on minimizing the variance of the new estimate without using the forgetting factor; and 3) on minimizing the variance of the new estimate using the forgetting factor.

B. Experimental Evaluation

We have also conducted experiments to evaluate the different position estimation algorithms developed in Section IV-A. In our experiments, a mobile TV camera (with a resolution of 256×256 and a lens focal length of $f = 16$mm) was used at each measurement point on a desired trajectory to acquire an image of a circular landmark of radius $R = 107$ mm. The camera usually recorded an image of an ellipse, which was sent via a TV communication link to the optical processor (see Fig. 4). The TV image of the ellipse was displayed on a liquid crystal device, and was read out by a laser beam. The coherent image of the ellipse was transformed optically by the HT filter, and the optical output in the parameter domain was detected by another TV camera interfaced to a microcomputer via an Image-100 image-processing board. A typical picture of the output is shown in Fig. 6. The parameters of the ellipse were determined from the detected image of the parameter domain along the two columns of $\theta = 0°$ and $\theta = 90°$ (see (8)). This computation was performed at very high speed, since it only involves very simple algorithm applied to a small number of points along the image in the parameter domain. The parameters of the ellipse were then used to determine the real position of the mobile system by employing the different algorithms without introducing any mobile system errors.

There are several error sources involved in our experiments: camera positioning errors (e.g., the positioning accuracy of the mobile TV camera is on the order of 1 mm), limited resolution of the Hough transform filter (128×128), parameter measuring errors (e.g., digitization error), and calibration errors.

The path taken in our experiment is a straight line path from (990, 2196) to (1705, 1475). We have plotted the position estimation error of two points on the trajectory to compare the three algorithms. The results from computer simulation and experiment are represented in Fig. 8(a) and (b), respectively, along with the results of the simple measurement. From Fig. 8, we can observe that 1) the algorithm based on minimizing the variance of the new estimate gives the best performance, and 2) all algorithms give a more accurate position estimate

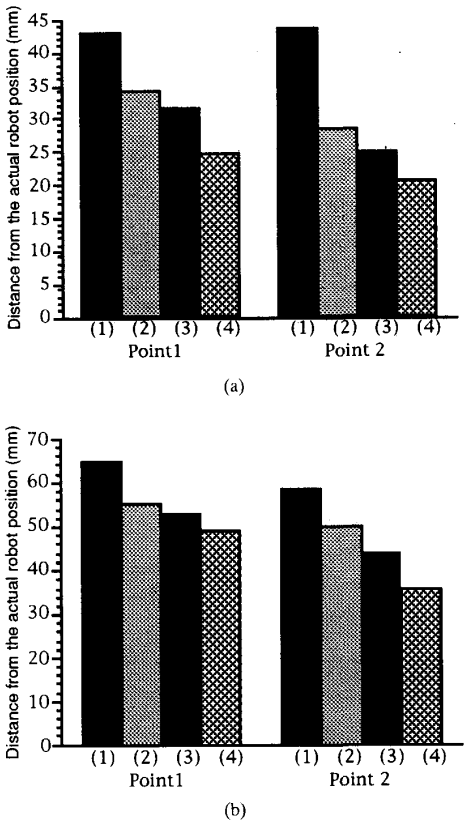

Fig. 8. Comparisons of error from the real position for different position estimation algorithms. (a) Computer simulation. (b) Experiment. At each point, from left to right, the algorithms are based on 1) simple measurement; 2) weighted average based on sensitivity; 3) least-squares method; and 4) minimizing the variance of the new estimate.

than the measurement.

C. Discussion of the Results

The computer simulation and the experimental results were found to be consistent. In the case of selecting the weights by minimizing the variance of the new estimate, we have considered both the sensitivity and the digitization errors by assuming a certain statistical error model. In most cases, it gives the best result. A moving window is introduced to compensate for the mobile system errors.

From the results in Figs. 7 and 8, we can conclude the following:

1) Each of the three navigation algorithms improve the navigation performance of the mobile system. This improvement will be even further enhanced when the distance traveled is increased.
2) The algorithm based on minimizing the variance of the new estimate with a moving window performs the best in the presence of both measurement and mobile system errors.
3) The algorithm based on minimizing the variance of the new estimate is the most efficient in compensating for measurement errors.
4) The experimental results are mostly consistent with the computer simulation.
5) The computer simulation and the experimental results show that the performances of the mobile system depend on the particular region passed by the mobile system as well as the locations where the measurements are made.

VI. Conclusion

A mobile system with a hybrid optoelectronic processor was studied. This processor combines the speed of optical image processing with the accuracy of digital computing to execute real-time navigation with sufficient accuracy. We analyzed different error sources that affect the navigation of the mobile system. To assure robust and accurate operation of the mobile system, we developed several algorithms based on different optimization criteria. Computer simulations and experiments were conducted to evaluate the performance of different algorithms. The results of the computer simulation and the experiments are consistent. The most accurate navigation performance of the mobile system is obtained with the algorithm based on minimizing the variance of the new estimate with a moving window.

Appendix I
The Relationship Between Landmark Image Parameters and Positions

In this Appendix, we derive the relationship between the circular landmark image parameters (i.e., the ellipse axes A_x and A_y) and the relative positions (r and α) in the 2-D case.

From Fig. 9(a), since triangles $\triangle ODE$ and $\triangle OC_iD_i$ are similar, we obtain $C_iD_i/f = R\cos\alpha/(r + R\sin\alpha)$; $\triangle OFB$ is similar to $\triangle OC_iB_i$, thus $C_iB_i/f = R\cos\alpha/(r - R\sin\alpha)$. Since $A_x = C_iD_i + C_iB_i/2$, we obtain

$$A_x = \frac{frR\cos\alpha}{r^2 - R^2\sin^2\alpha}. \tag{34}$$

The $\triangle OGH$ and $\triangle OG_iH_i$ of Fig. 9(b) are similar, so that $(2A_y/f) = (2R/r)$, or

$$A_y = \frac{fR}{r}. \tag{35}$$

From (34) and (35), we get (1).

Appendix II
Development of the Algorithm Based on Least-Square Errors

The mean square error can be expressed as

$$J = \sum_{i=1}^{n}(\bar{r}^n - r_i^n)^2 = \sum_{j=1}^{n}\left(r_j^n - \frac{\sum_{i=1}^{n}(w_r^r)_i^2 r_i^n}{\sum_{i=1}^{n}(w_r^r)_i}\right)^2.$$

To determine the minimum, we should set the derivative of J with respect to w_k^r to zero:

$$\frac{\partial J}{\partial w_k^r} = 0$$

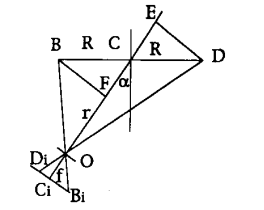

(a)

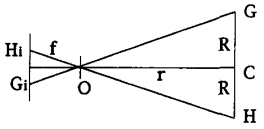

(b)

Fig. 9.

that is

$$\sum_{i=1}^{n}(r_k^n - r_i^n)w_i^r = 0.$$

What we have is a homogeneous linear system of equations; to avoid a trivial solution, we have to pick one weight first. Here we take the measurement in the highest sensitivity region as having a weight of 1. In order to achieve real-time operation, we can also use the recursive method to solve the equations approximately.

ACKNOWLEDGMENT

We appreciate the efforts of Mr. Harry Alter from the DOE in coordinating the University Program in Robotics for Advanced Reactors. Discussions with Dr. Johann Borenstein, The University of Michigan, are greatly appreciated.

REFERENCES

[1] E. S. McVey, K. C. Drake, and R. M. Inigo, "Range measurements by a mobile robot using a navigation line," *IEEE Trans. Pattern Anal. Machine Intell.*, vol. PAMI-8, pp. 105–109, Jan. 1986.

[2] T. Takeda, A. Kato, T. Suzuki, and M. Hosoi, "Automated vehicle guidance using spotmark," in *Proc. IEEE Int. Conf. Robotics Automat.*, vol. 2, pp. 1349–1353, 1986.

[3] M. H. E. Larcombe, "Tracking stability of wire guided vehicle," in *Proc. 1st Int. Conf. Automat. Guided Vehicle Syst.*, June 1981, pp. 137–144.

[4] S. T. Barnard and M. A. Fischler, "Computational stereo," *Comput. Survey*, vol. 14, pp. 553–572, Dec. 1982.

[5] J. W. Courtney, M. J. Magee, and J. K. Aggarwal, "Robot guidance using computer vision," *Pattern Recognition*, vol. 17, no. 6, pp. 585–592, 1984.

[6] D. Nitzan, "Three-Dimensional Vision Structure for Robot Applications," *IEEE Trans. Pattern Anal. Machine Intell.*, vol. 10, no. 3, pp. 301–309, 1988.

[7] M. J. Magee and J. K. Aggarwal, "Determine the position of a robot using a single calibration object," *CH2008-1/84*, pp. 140–149, 1984.

[8] K. Sugihara, "Some location problems for robot navigation using a single camera," *Computer Vision, Graphics, and Image Processing*, vol. 42, no. 1, pp. 112–121, 1988.

[9] E. Krotkov, "Mobile robot localization using a single image," in *Proc. 1989 IEEE Int. Conf. Robotics Automat.*, 1989, pp. 978–983.

[10] C. D. McGillem and T. S. Rappaport, "Infra-red location system for navigation of automated vehicles," in *Proc. IEEE Int. Conf. Robotics Automat.*, vol. 3, 1988, pp. 1236–1238.

[11] K. Nishide, M. Hanawa, and T. Kondo, "Automatic position findings of vehicle by means of laser," *Proc. 1986 IEEE Int. Conf. Robotics Automat.*, vol. 2, 1986, pp. 1343–1348.

[12] T. Tsumura and M. Hashimoto, "Positioning and guidance of ground vehicle by use of laser and corner cube," in *Proc. 1986 IEEE Int. Conf. Robotics Automat.*, vol. 2, 1986, pp. 1335–1342.

[13] M. R. Kabuka and A. E. Arenas, "Position verification of a mobile robot using standard pattern," *IEEE J. Robotics Automat.*, vol. RA-3, pp. 505–516, Dec. 1987.

[14] I. Fikui, "TV image processing to determine the position of a robot vehicle," *Pattern Recog.*, vol. 14, no. 6, pp. 101–109, 1981.

[15] C.-N. Shyi, J.-Y. Lee, and C.-H. Chen, "Robot guidance using standard mark," *Electron. Lett.*, vol. 24, no. 21, pp. 1326–1327, 1988.

[16] J.-D. Lee, J.-Y. Lee, C.-H. Chen, and Y.-Y. Sun, "A new approach to robot guidance in an unfamiliar environment using indication-post," in *Proc. 1989 IEEE Int. Conf. Robotics Automat.*, vol. 3, 1989, pp. 1433–1438.

[17] C. M. Wang, "Location estimation and uncertainty analysis for mobile robots," in *Proc. 1988 IEEE Int. Conf. Robotics Automat.*, vol. 3, 1988, pp. 1230–1235.

[18] R. McKandall and M. Mintz, "Robust fusion of location information," robots," in *Proc. 1988 IEEE Int. Conf. Robotics Automat.*, vol. 3, 1988, pp. 1239–1243.

[19] R. C. Luo, M.-H. Lin, and R. S. Scherp, "Dynamic multi-sensor data fusion system for intelligent robots," *IEEE J. Robotics Automat.*, vol. 4, pp. 386–396, 1988.

[20] H. F. Durrant-Whyte, "Sensor models and multisensor integration," *Int. J. Robotics Res.*, vol. 7, no. 6, pp. 97–113, 1988.

[21] A. M. Flynn, "Combining sonar and infrared sensors for mobile robot navigation,"*Int. J. Robotics Res.*, vol. 7, no. 6, pp. 5–14, 1988.

[22] J. M. Richardson and K. A. Marsh, "Fusion of multisensor data," *Int. J. Robotics Res.*, vol. 7, no. 6, pp. 78–96, 1988.

[23] R. C. Smith and P. Cheeeseman, "On the representation and estimation of spatial uncertainty,"*Int. J. Robotics Res.*, vol. 7, no. 6, pp. 56–68, 1988.

[24] P. Ambs, Y. Fainman, S. H. Lee, and J. Gresser, "Computerized design and generation of space-variant holographic filters," *Appl. Opt.*, vol. 27, pp. 4753–4760, Nov. 1988.

[25] H. Stark and J. W. Woods, *Probability, Random Processes, and Estimation Theory for Engineers*. Englewood Cliffs, NJ: Prentice-Hall, 1986, chs. 2 and 3.

[26] J. Borenstein and Y. Koren, "Motion control analysis of a mobile robot," *J. Dyn. Syst., Meas., Contr.*, vol. 109, pp. 73-79, June 1987.

[27] ——, "A mobile platform for nursing robots," *IEEE Trans. Ind. Electron.*, vol. IE-2, pp. 158-165, May 1985.

[28] L. G. Parratt, *Probability and Experimental Errors in Science*. New York: Wiley, 1961, ch. 3.

[29] H. V. Poor, *An Introduction to Signal Detection and Estimation*. New York: Springer-Verlag, 1988, ch. 5.

[30] G. C. Goodwin and K. S. Sin, *Adaptive Filtering, Prediction, and Control*. Englewood Cliffs, NJ: Prentice-Hall, 1984, ch. 3.

Liqiang Feng received the B.S. degree in automotive engineering in 1985 from Tsinghua University, Beijing, People's Republic of China, and the M.S. degree in mechanical engineering in 1988 from the University of Michigan, Ann Arbor, where he is currently a Ph.D. candidate in mechanical engineering. His dissertation research concentrates on adaptive motion control of mobile robots, mobile robot navigation, and optical information processing.

Yeshaiahu Fainman received the master's degree in electrical engineering in 1979 and the Ph.D. degree in 1983 from the Technion—Israel Institute of Techology, Haifa, Israel.

He is an Associate Professor in the Department of Electrical and Computer Engineering at the University of California, San Diego. From 1988 to 1990 he was an Associate Professor in the Department of Mechanical Engineering and Applied Mechanics, College of Engineering, of the University of Michigan, Ann Arbor. From 1983 to 1988, he was an Assistant Research Physicist at the University of California, San Diego. His research interests are in optical information processing, holography, and photorefractive optics. He has published more than 35 papers and contributed a chapter to a book in the field. He has received various honors and awards.

Dr. Fainman is a member of OSA and SPIE.

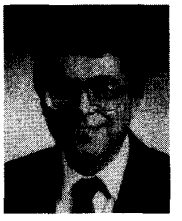

Yoram Koren (M'76–SM'88) received the B.Sc. and M.Sc. degrees in electrical engineering and the D.Sc. degree in mechanical engineering in 1970 from Technion—Israel Institute of Technology, Haifa.

He is a Professor in the Department of Mechanical Engineering at the University of Michigan, Ann Arbor. He has 22 years of research, teaching, and consulting experience in the automated manufacturing field. He is the author of more than 120 technical papers and three books. He is the inventor of three U.S. patents in robotics. His books, *Robotics for Engineers* (McGraw Hill, 1985) was translated into Japanese and French.

Dr. Koren is a Fellow of the ASME, and Active Member of CIRP, and a Fellow of the SME/Robotics-International.